Available online at www.sciencedirect.com
SCIENCE DIRECT®
Journal of Solid State Chemistry 177 (2004) 1388–1392
JOURNAL OF SOLID STATE CHEMISTRY
http://elsevier.com/locate/jssc

$SmCuS_2$: crystal structure refinement, electrical, optical and magnetic properties

Jaime Llanos,[a,*] Carlos Mujica,[a] Víctor Sánchez,[a] Walter Schnelle,[b] and Raúl Cardoso-Gil[b]

[a] *Departamento de Química, Universidad Católica del Norte, Avda. Angamos 0610, Casilla 1280 Antofagasta, Chile*
[b] *Max-Planck-Institut für Chemische Physik fester Stoffe, Nöthnitzer Str. 40, 01187 Dresden, Germany*

Received 7 August 2003; received in revised form 4 November 2003; accepted 23 November 2003

Abstract

The ternary copper(I) samarium(III) sulfide $SmCuS_2$ has been prepared by heating SmS and CuS in the ratio 1:1 at 1273 K for 3 days in sealed quartz ampoule. Single-crystal diffraction analysis shows that $SmCuS_2$ crystallizes monoclinic in the $LaCuS_2$ structure-type ($P2_1/c$ (No. 14); $a = 647.15(3)$ pm, $b = 710.82(3)$ pm, $c = 677.96(3)$ pm and $\beta = 98.353(4)^\circ$; $Z = 4$) and it is isostructural to $PrCuS_2$. According to electrical conductivity as well as diffuse reflectance measurements, $SmCuS_2$ is a semiconductor with an optical band gap of 2.1 eV. The magnetic susceptibility data show that Sm moments in $SmCuS_2$ orders antiferromagnetically at 2.92(6) K.

Keywords: Chalcogenides; Inorganic compounds; Semiconductors; Chemical synthesis; Impedance spectroscopy; X-ray diffraction; Single crystal; Electrical properties; Magnetic properties; Optical properties

1. Introduction

Since the first works published by Julien-Pouzol et al. [1–2] many efforts have been made to prepare and characterize ternary lanthanide copper sulfides. However, only a few of such ternary rare-earth copper sulfides have been structurally fully characterized by means of X-ray diffraction methods. Single crystal X-ray diffraction analysis have been carried out for $LaCuS_2$, $YCuS_2$ and $PrCuS_2$, whereas the crystal structure of $NdCuS_2$ has been refined from X-ray powder diffraction data by the Rietveld method [3–6]. For the others members of the $LnCuS_2$ series (Ln = Gd, Dy, Ho, Yb, Lu) only the lattice parameters have been reported. The phases containing Ln = La, Nd; Sm and Gd, crystallize monoclinic in the space group $P2_1/c$ (No. 14), while those of the heavier rare-earth and yttrium crystallize orthorhombic in the space group *Pnma* (No. 62). $LuCuS_2$ is unique in the series, occurring in both orthorhombic and hexagonal system, with the hexagonal phase of $LuCuS_2$ being isostructural to $ScCuS_2$, which crystallizes in the space group $P3m1$ (No. 156) [7].

The interest in these compounds is related to their physical and chemical properties which are promising for applications such as magnetic storage materials and possible as photovoltaic materials for solar energy conversion [8–10].

In the present work, we have undertaken an investigation of the electrical and magnetic properties, optical band gap determination, as well as the full crystal structural refinement from single-crystal intensity data for the monoclinic phase $SmCuS_2$. This compound was already described in 1984 by Guseinov et al., however, the available structural characterization is no longer state of the art [11].

2. Experimental

2.1. Synthesis

The compound $SmCuS_2$ was prepared from synthetic SmS and CuS (Aldrich, 99 + %). The starting materials

*Corresponding author. Fax: +56-55-355-632.
E-mail address: jllanos@ucn.cl (J. Llanos).

0022-4596/$ - see front matter © 2003 Elsevier Inc. All rights reserved.
doi:10.1016/j.jssc.2003.11.018

were loaded in a glove box into quartz tubes subsequently sealed in vacuum (13×10^{-3} Pa). The ampoules were heated at 1273 K for 72 h and then allowed to cool down to room temperature over a period of 5 days. Inspection of the product showed some brown-reddish crystals among a dark red bulk. Both, crystals and bulk material consist of a single phase according to the X-ray powder diffraction analysis.

SmS was prepared by reducing Sm_2S_3 with metallic Sm at 873 K under vacuum, followed by heating at 1200 K to remove excess of Sm. The parent compound Sm_2S_3 was prepared heating Sm_2O_3 in an alumina crucible at 900 K under continuos flow of CS_2 using Ar as carrier gas. After 20 h, the X-ray powder pattern of the product can be fully indexed as Sm_2S_3, no diffraction lines of Sm_2O_3 were observed within the detection limit of this analytic method.

2.2. X-ray powder diffraction

The samples were analyzed using a Siemens D-5000 powder diffractometer equipped with graphite monochromator, using Cu$K\alpha$ radiation ($\lambda = 154.057$ pm). α-quartz was used as internal standard. For qualitative comparison of the experimental powder pattern, theoretical patterns were calculated from single crystal data using the program Lazy-Pulverix [12]. The lattice parameters were determined from X-ray powder data (Huber Guinier image plate camera G670, Co$K\alpha_1$ $\lambda = 178.896$ pm) by a least-square refinement of the 2θ values for 82 reflections in the range $10° < 2\theta < 100°$ using the program package WinCSD [13]. LaB_6 was used as an internal standard ($a = 415.695(6)$ pm).

2.3. Crystal structure determination

A well-shaped single crystal of $SmCuS_2$ was selected and mounted on a glass capillary. Intensity data were collected on an STOE-IPDS diffractometer equipped with graphite monochromator and using Ag$K\alpha$ radiation. Numerical absorption correction was performed with optimized shape of the crystal [14]. The structure was solved using SHELXS-97 [15] resulting in agreement with the $LaCuS_2$ structure [3]. The subsequent refinement was performed with SHELXL-97 [15].

The refinement in the $LnCuSe_2$ structure results in a relative large U_{eq} value for the Cu atom giving us a hint of disorder on the this position [16]. This finding is normal for d^{10} ions, according to the results reported in Refs. [17,18]. This observation is even supported through the relatively high residual electron density located near Cu, not corrected by the applied harmonic model. Crystallographic data and experimental conditions are listed in Table 1, atomic positions and displacement parameter are shown in Table 2.

2.4. Magnetic measurements

The magnetization was measured in a SQUID-magnetometer (MPMS XL7, Quantum Design) in external fields between 70 kOe and 100 Oe and temperatures between 1.8 and 400 K.

2.5. Conductivity measurements

The electrical conductivity measurement was carried out using the electrochemical impedance spectroscopy

Table 1
Crystallographic data and details of the crystal structure analysis

Formula; molar mass	Sm Cu S_2; 278.0 amu
Crystal	Red-brown prism; $0.10 \times 0.09 \times 0.07$ mm
Space group; formula units	$P2_1/c$ (No.14); $Z = 4$
Unit cell (294 K)	$a = 647.15(3)$ pm
	$b = 710.82(3)$ pm
	$c = 677.96(3)$ pm
	$\beta = 98.353(4)°$
Volume; density	$308.56(1) \times 10^6$ pm^3; 5.985 g cm^{-3}
Data collection	STOE-IPDS; Ag$K\alpha$ radiation ($\lambda = 56.086$ pm, graphite monochromator), 120 exposures, $\Delta\varphi = 1.5°$
Structure refinement	SHELXS-97, SHELXL-97 [15]
	Full-matrix least-squares on F^2 (38 parameter)
Absorption correction	Numerical ($\mu = 141.3$ cm^{-1}) [14]
Min. and max. transmission	0.2893, 0.4546
Measured/unique reflections	4310/1194
R_{int}	0.0275
Measured range	$5.02° \leqslant 2\theta \leqslant 51.54°$
	$-9 \leqslant h \leqslant 9, -10 \leqslant k \leqslant 10, -10 \leqslant l \leqslant 10$
Observed reflections ($F_o > 4.0\ \sigma(F_o)$)	1052
$R(F)$; w$R2$	0.0237/0.0519
Goof = S =	1.078
$\Delta\rho_{max}$	3.62 e Å^3
$\Delta\rho_{min}$	−3.04 e Å^3

Table 2
Positional and equivalent displacement parameters U_{eq} and U_{ij} (in pm^2) for $SmCuS_2$

Atom	Position	x	y	z	S.O.F.	U_{eq}
Sm	4*e*	0.30683(3)	0.05142(3)	0.19725(3)	1.000	57(1)
Cu	4*e*	0.08809(11)	0.65574(11)	0.06171(11)	1.000	179(2)
S1	4*e*	0.57828(17)	0.27193(16)	0.00030(15)	1.000	56(2)
S2	4*e*	0.08924(17)	0.38443(16)	0.28228(16)	1.000	68(2)
	U_{11}	U_{22}	U_{33}	U_{23}	U_{13}	U_{12}
Sm	62(1)	49(1)	61(1)	−4(1)	10(1)	−7(1)
Cu	153(3)	158(3)	241(3)	−55(3)	87(2)	−38(3)
S1	59(4)	53(4)	54(4)	−1(3)	5(3)	−4(3)
S2	68(4)	66(4)	68(4)	−2(3)	0(3)	9(4)

Standard deviations are given in parentheses. The anisotropic displacement factor exponent take the form: $[-2\pi^2(h^2a^{*2}U_{11} + \cdots + 2hka^*b^*U_{12})]$.

(EIS) technique from room temperature to 450 K. The applied signal amplitude was 10 mV in the frequency range of 10^{-2}–1 kHz. A cylindrical pellet ($\phi = 6$ mm) was pressed from powders of $SmCuS_2$. The impedance measurement was performed in a conductivity cell provided with two identical electrodes. The two opposite flat surfaces of the samples were sputtered with gold and placed between the gold electrodes. For this measurement a VoltaLab40 PGZ301 universal potentiostat was used.

2.6. Optical properties

The diffuse reflectance UV–Vis spectrum was recorded using a Perkin-Elmer Lambda 20 UV–Vis spectrophotometer equipped with a Labsphere RSA-PE-20 diffuse reflectance accessory. Magnesium oxide was used as a reference and the spectrum was recorded in the range of 1.5–6.0 eV at room temperature. Reflectance measurement was converted to absorption spectrum using the Kubelka-Munk function $F(R_\infty)$.

3. Results and discussion

$SmCuS_2$ crystallizes in the $LaCuS_2$ structure [3], whose main characteristic is the presence of $[CuS_4]^{7-}$ tetrahedra which condense by pairs sharing a common edge ($[Cu_2S_6]^{10-}$) (see Fig. 1); at the same time, they are connected to each other sharing corners through S(1) to build up undulated layers $_\infty{}^2\{[Cu(S)_{3/3}(S)_{1/1}]^{3-}\}$ parallel to (100). Their three-dimensional cross-linkage is achieved by the rare-earth cation in a monocapped trigonal prismatic coordination of seven S^{2-} anions (see Fig. 2).

Trying to understand the "anomalous" displacement parameter of Cu in the refinement (see Fig. 1), it was found in the reported results of the structure refinement of $LaCuS_2$ [3] and $PrCuS_2$ [5], that the anisotropy of Cu is also systematically present in these isotypes and, like

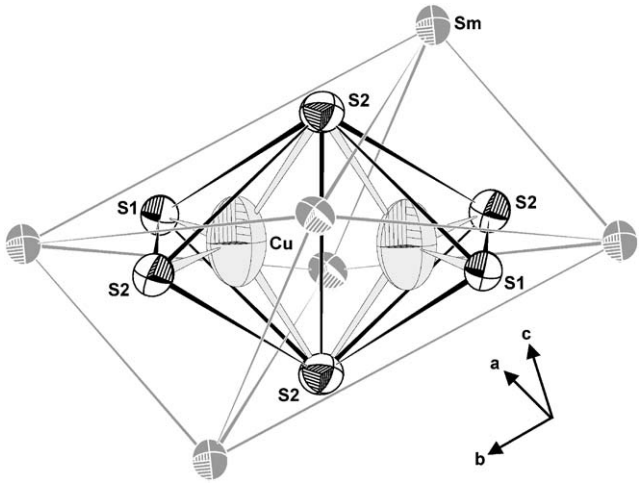

Fig. 1. Coordination of Cu with thermal ellipsoids (drawn with 99.9% probability) in a double tetrahedron (bond lines between Sm atoms were drawn for clarity).

in $SmCuS_2$, the thermal ellipsoids are elongated parallel to the common edge of the double tetrahedra. In order to determine effectively if the anisotropy of Cu obey to a thermal vibration, X-ray single crystal analysis at different temperatures are in progress.

Considering the distortion of both polyhedra of Sm and Cu, all seven Sm–S distances in the coordination sphere are different and range from 280.1(1) to 299.7(1) pm. The Cu–S distances are also different and vary from 231.9(1) to 246.5(1) pm. Selected interatomic distances are listed in Table 3.

The UV–Vis spectra of $SmCuS_2$ is shown in Fig. 3. The optical band gap (E_g) corresponds to the intersection point between the base line along the energy axis and the extrapolated line from the linear portion of the threshold. Thus, E_g can be assessed to be 2.1 eV a typical value for semiconducting materials and consistent with the red–brown color of the sample.

The electrical conductivity of $SmCuS_2$ as a function of temperature is shown in Fig. 4. The room-temperature

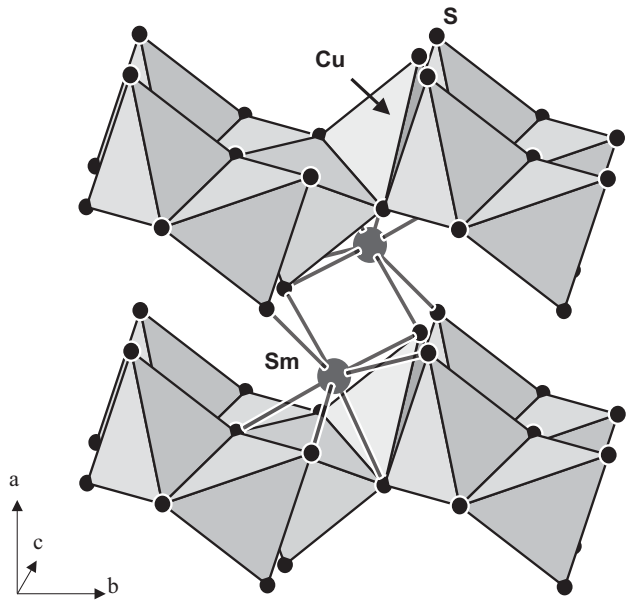

Fig. 2. Projection long [001] of the crystal structure of $SmCuS_2$. Some Sm atoms are omitted for better visualization.

Table 3
Interatomic distances (in pm). Standard deviations are given in parentheses

Cu–S(1)	231.7(1)
Cu–S(2)	233.0(1)
Cu–S(2)	244.0(1)
Cu–S(2)	246.2(1)
Cu–Cu	257.4(2)
S(1)–Cu	231.7(1)
S(1)–Sm	280.0(1)
S(1)–Sm	281.4(1)
S(1)–Sm	283.0(1)
S(1)–Sm	287.4(1)
S(2)–Cu	233.0(1)
S(2)–Cu	244.0(1)
S(2)–Cu	246.2(1)
S(2)–Sm	284.6(1)
S(2)–Sm	285.6(1)
Sm–S(1)	279.9(1)
Sm–S(1)	281.4(1)
Sm–S(1)	283.0(1)
Sm–S(2)	284.6(1)
Sm–S(2)	285.6(1)
Sm–S(1)	287.4(1)
Sm–S(2)	299.2(2)
Sm–Cu	322.0(1)
Sm–Cu	331.1(1)
Sm–Cu	355.6(1)
Sm–Cu	355.6(1)
Sm–Sm	398.5(1)

conductivity $\sigma(300\,\mathrm{K})$ of the sample is $6.3\times10^{-4}\,\mathrm{S\,cm^{-1}}$ and increases with the temperature ($\sigma(450\,\mathrm{K})=6.3\times10^{-3}\,\mathrm{S\,cm^{-1}}$). This behavior, besides the usual electron

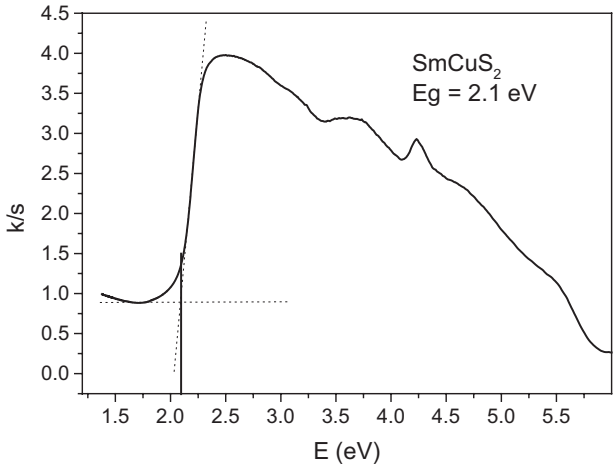

Fig. 3. Diffuse reflectance spectrum of $SmCuS_2$ after a Kubelka-Munk transformation ($T=298\,\mathrm{K}$).

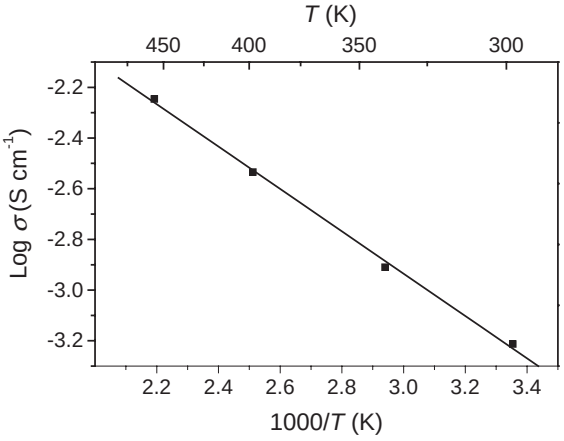

Fig. 4. Temperature dependence of the electrical conductivity of $SmCuS_2$.

counting rules are consistent with the semiconductor character of the sample.

$SmCuS_2$ shows typical magnetic susceptibility behavior for a $4f^5$ ion of Sm^{3+}, i.e., no Curie–Weiss law but a curved $1/\chi(T)$ (see. Fig. 5), with a maximum between ca. 280 and 400 K, here it is found at ca. 370 K. Cu carries no magnetic moment, i.e., it is a $3d^{10}$ configuration corresponding to Cu^{1+}. Sm^{3+} moments order antiferromagnetically at 2.92(6) K which is seen from susceptibility $\chi(T)$ in relatively high fields. In lower fields a weak ferromagnetic signal is observed, which means that the Sm^{3+} moments are not fully compensated (weak ferromagnetism from canted moments). The isothermal magnetization curve shows a hysteresis with low remanent moment ($0.024\,\mu_B$/Sm-atom) and asymmetric coercive fields ($+700$ Oe or -1300 Oe, depending on polarity change). Also the virginal curve is outside the last segment of the full hysteresis. Only the coincidence with the small antiferromagnetic signal at

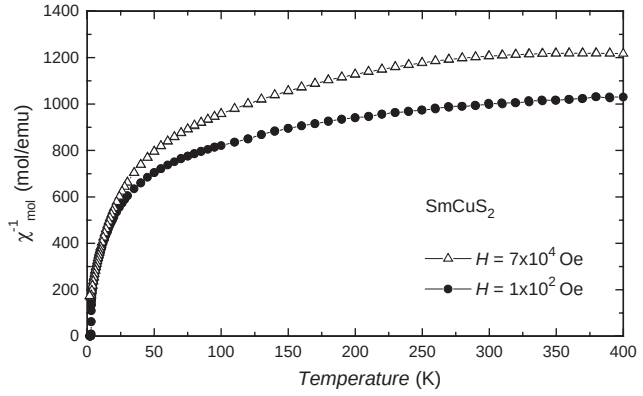

Fig. 5. Temperature dependence of the inverse magnetic susceptibility $\chi^{-1}(T)$ of $SmCuS_2$ as measured in magnetic fields of 1×10^2 and 7×10^4 Oe.

higher fields suggests that this weak ferromagnetism is intrinsic and not due to an impurity. A low-temperature Curie–Weiss fit (4–9 K) is consistent with a small antiferromagnetic interaction of order -2 to -4 K.

Acknowledgments

This work was supported by FONDECYT Contract 1020440. The authors acknowledge fruitful discussions with Dr. H. Borrmann and Dr. W. Carrillo-Cabrera.

References

[1] M. Julien-Pouzol, M. Guittard, C. Adolphe, C. R. Acad. Sci. 267 (1968) 823.
[2] M. Julien-Pouzol, M. Guittard, Ann. Chim. 7 (1972) 253.
[3] M. Julien-Pouzol, S. Jaulmes, A. Mazurier, M. Guittard, Acta Crystallogr. B 37 (1981) 1901.
[4] P. Lauxmann, T. Schleid, Z. Anorg. Allg. Chem. 626 (2000) 1608.
[5] P. Lauxmann, S. Strobel, T. Schleid, Z. Anorg. Allg. Chem. 628 (2002) 2403.
[6] Y. Wang, N. Sato, T. Fujino, Mater. Res. Bull. 36 (2001) 1029.
[7] T. Murugesan, J. Gopalakrishnan, Indian J. Chem. A 22 (1983) 469.
[8] T. Ohtani, Y. Miyoshi, Y. Fujii, T. Koyakumaru, T. Kusano, K. Minami, Solid State Commun. 120 (2001) 95.
[9] J.J. Laferski, in: G.G. Libowitz, M.S. Wittingham (Eds.), Material Science in Energy Technologie, Academic Press, New York, 1979, p. 248.
[10] E.P. Wohlfarth, in: E.P. Wohlfarth (Ed.), Ferromagnetic Materials, North- Holland, New York, 1980, p. 1.
[11] G.G. Guseinov, A.S. Amirov, I.R. Amiraslanov, K.S. Mamedov, Dokl. Akad. Nauk Az. SSR 40 (1984) 62.
[12] K. Yvon, W. Jeitschko, E. Pahrté, J. Appl. Crystallogr. 10 (1977) 73.
[13] L.G. Akselrud, P.Yu. Zavalli, Yu. Grin, V.K. Pecharsky, B. Baumgartner, E. Wölfel, Mater. Sci. Forum 335 (1993) 133.
[14] X-Shape 1.03, Crystal Optimization for Numerical Absorption Correction, Stoe & Cie GmbH, Darmstadt, Germany, 1998.
[15] G.M. Sheldrick, SHELXS-97, SHELXL 97, University of Göttingen, 1997.
[16] I. Ijjaali, K. Mitchell, J.A. Ibers, J. Solid State Chem. (2003) (available in Science Direct), in press.
[17] A. Vanderlee, F. Boucher, M. Evain, R. Brec, Z. Kristallogr. 203 (1993) 247.
[18] E. Durand, G. Ouvrard, M. Evain, R. Brec, Inorg. Chem. 29 (1990) 4916.